CHAPTER - 2

THEORETICAL BACKGROUND

2.1 Theories of liquid crystalline phases

The theories of liquid crystalline phases have been described in detail in several books [1-5]. I am giving below, the salient features of the mean-field theories of nematic and smectic A phases as developed by Maier-Saupe [6] and McMillan [7,8] respectively.

2.1.1 Maier-Saupe mean field theory of nematic phase of rod like molecules

In Chapter 1 it has been mentioned that the rod like molecules of a liquid crystalline substance tend to align their long axes along a preferred direction, called the director $\vec{n}$, below a certain temperature. The problem of the nematic phase (N) and the Nematic-Isotropic (N-I) transition has been successfully solved in 1959 by Maier and Saupe. They assumed that the molecular force of the induced dipole-induced dipole type (i.e anisotropic dispersive force) between two neighbouring molecules is primarily responsible for this phase. The distribution of the molecular long axes about the director is given by an orientational distribution function $f(\cos\theta)$, assuming cylindrical symmetry of the mesophase, where θ is the angle between the director and the molecular long axis. Since the molecules within the system have no head to tail asymmetry, then $\vec{n} = -\vec{n}$, and $f(\cos\theta)$ is an even function of $\cos\theta$. The distribution function can also be written as [9]:

$$f(\cos\theta) = \sum_{L \text{ even}} (2L+1)/2 \, \langle P_L(\cos\theta) \rangle \, P_L(\cos\theta) \qquad 2.1$$

where $P_L(\cos\theta)$ are the L^{th} even order Legendre polynomials, and

$\langle P_L(\cos\theta)\rangle$ are the statistical average given by

$$\langle P_L(\cos\theta)\rangle = \int_0^1 P_L(\cos\theta)\, f(\cos\theta)\, d(\cos\theta) \Big/ \int_0^1 f(\cos\theta)\, d(\cos\theta) \qquad 2.2$$

$\langle P_L\rangle$ are called the orientational order parameters, of which the first member, i.e, $\langle P_2\rangle$ is commonly called the order parameter. This order parameter gives the measure of how well aligned the molecules are in a nematic phase. $\langle P_2\rangle$ is equal to one for perfectly oriented sample and is equal to zero for randomly oriented, i.e, isotropic liquid.

A phenomenological expression for the mean field can be written as follows. The average field should be such that the potential of the molecule under study should be minimum when it makes θ =0 with $\hat{n}$ i.e., the mean field would tend to rotate the molecules towards $\hat{n}$. Secondly the torque of the mean field should be more, more aligned are the molecules in the system. On these two considerations the potential energy of a molecule making an angle θ with the director $\hat{n}$ is [6]

$$V(\cos\theta) = v\langle P_2\rangle\, P_2(\cos\theta) \qquad 2.3$$

where v is the coupling constant.
Hence, the orientational distribution function $f(\cos\theta)$ and the partition function Z are given by,

$$f(\cos\theta) = Z^{-1} \exp\left[-V(\cos\theta)/kT\right] \qquad 2.4$$

$$Z = \int_0^1 \exp\left[-V(\cos\theta)/kT \right] d(\cos\theta) \qquad 2.5$$

k being the Boltzmann constant.
Substituting the value of $f(\cos\theta)$ as in equation (2.4) to

equation (2.2), we get for L = 2

$$\langle P_2 \rangle = Z^{-1} \int_0^1 P_2(\cos\theta) \exp [\langle P_2 \rangle P_2(\cos\theta)/T^*] \, d(\cos\theta) \qquad 2.6$$

where $T^* = v/kT$

From the principle of ergodicity it is seen from equation (2.6) that the time average, (i.e. order of a particular molecule averaged over sufficiently long time) is equal to the ensemble average (i.e. the average over all other molecules) and a self consistent solution of it is sought. For all values of T^* (or T) $\langle P_2 \rangle = 0$ is a solution, while for $T^* < .22284$,two other solutions of $\langle P_2 \rangle$ appear. Obviously, the state with minimum free energy is the stable one. It can be shown that for $T^* < .22019$, a state with $\langle P_2 \rangle > 0$ is stable one, which can be identified with nematic phase, whereas for $T^* > .22019$, $\langle P_2 \rangle = 0$, gives the equilibrium state, which is the isotropic liquid.

The nematic-isotropic liquid transition occurs at $T_c^* = 0.22019$ and $\langle P_2 \rangle_c = 0.4289$, according to the Maier Saupe theory. Thus, this transition is always of the first order. However, the N-I transition energy has been calculated to be around 0.83 cal/mole ^{o}K which pretty small compared to usual solid to liquid transition which is around 25 cal/mole^{o}K . This transition is therefore often called weakly first order transition. Values of $\langle P_2 \rangle$ as a function of T^* can be calculated easily by solving equation (2.6) iteratively. For many liquid crystals the Maier-Saupe $\langle P_2 \rangle$ values agree quite well with those found experimentally.

2.1.2. McMillan's theory for smectic A phase

In smectic A phase, there is a periodic density variation along the layer normal (z direction) in addition to the

orientational ordering of the molecular axes. Hence, the nomalised distribution function can be written, in this case, as

$$f(\cos\theta),z) = \sum_{L,\text{even}} \sum_{n} A_{L,n}\, P_L(\cos\theta)\, \cos\,(2\pi nz/d) \qquad 2.7$$

$$\text{with} \int_{-1}^{1} \int_{0}^{d} f(\cos\theta,z)\, dz\, d(\cos\theta) = 1 \qquad 2.8$$

as normalising condition, d being the layer thickness.

McMillan [7,8], following Kobayashi [10,11], assumed a model potential of the following form

$$V_M(\cos\theta,z)=-v[\, \delta\alpha\tau\, \cos(2\pi z/d) + \{\eta + \alpha\sigma\, \cos\,(2\pi z/d)\}\, P_2(\cos\theta)] \qquad 2.9$$

where α and δ are two parameters of the potential. $\eta=\langle P_2(\cos\theta)\rangle$, $\tau=\langle\cos(2\pi z/d)\rangle$ and $\sigma=\langle P_2(\cos\theta)\ \cos(2\pi z/d)\rangle$ are the orientational, translational and mixed order parameters respectively, and $\langle..\rangle$ denotes statistical average of the quantities inside.

The distribution function can be written as

$$f_M(\cos\theta,z) = Z^{-1}\, \exp\,[\, -V_M(\cos\theta,z)/kT\,] \qquad 2.10$$

where the partition function

$$Z = \int_0^1 \int_0^d \exp\,[\, -V_M\,(\,\cos\theta,z)/kT]\, d(\cos\theta)\, dz \qquad 2.11$$

Once again, three self consistency equations containing η,τ and σ can be written and solved iteratively.

Out of several solutions, the equilibrium state is identified by the minimum value of free energy.

In general, we get the following three cases:

Case I: $\eta = 0$, $\tau = 0$, $\sigma = 0$, isotropic liquid.
Case II: $\eta \neq 0$, $\tau = 0$, $\sigma = 0$, nematic liquid crystal.
Case III: $\eta \neq 0$, $\tau \neq 0$, $\sigma \neq 0$, smectic liquid crystal.

While nematic-isotropic transition is always first order, the smectic A - nematic transition can be either first order ($T_{AN}/T_{NI} > 0.88$) or second order ($T_{AN}/T_{NI} < 0.88$), where T_{AN} and T_{NI} are the smectic A- nematic and nematic-isotropic transition temperatures respectively.

2.2 Identification of phases

2.2.1 Texture studies

The most striking feature of liquid crystals is the wide variety of visual patterns they display under polarised light. These patterns called textures are due almost entirely to the defect structure that occurs in the long-range molecular order of the liquid crystalline materials. Appearing under the polarizing microscope as ell ipses, parabolas, hyperbolas, lines and points, colourful structural singularities are understood through topological and geometrical arguments. For the determination of transition temperatures and the identification of liquid crystalline phases, observation of textures is an important technique for the liquid crystal physicist. They are observed in thin layers ($\approx$ 10-20 micrometer) between two glass slides. Change in texture at a particular temperature indicates the occurrence of phase transition. For a given structure, different textures can exist, depending on the special conditions in preparations of the sample.

Homeotropic textures are occasionally observed in phases of nematic, smectic A, smectic B and other orthogonal smectic phases. In smectic C, smectic F and smectic I phases (all tilted smectic phases) broken focal conic texture are generally observed [12]. The in-layer ordered smectic phases often show mosaic texture. Classification of different liquid crystalline phases by the observation of textures alone is often ambiguous, and other methods are needed to support it. Detailed description of various textures, with photographs, is given by Demus and Richter [12].

2.3. X-ray diffraction from mesophases

Studies of the properties of liquid crystals and further developments in the theory of the liquid-crystalline state are based, first and foremost, on the results of structural investigations, and, in particular x-ray structure analysis. From x-ray experiment, the fourier image of the correlation density function can be determined, the reconstruction of which from the scattering data yields information both on the mutual arrangement of molecules in a liquid crystal and the specific features of the orientational and translational long range order. Different liquid-crystalline phases give different x-ray patterns. X-ray data enable the statistical functions characterizing various distortions of the initial crystal lattice to be determined [13,14], and give the parameters of the orientational order in a liquid crystal, the tilt of the molecules, and the electron density distribution in smectic layers [13-19].

Unoriented nematic phase shows x-ray diffraction pattern which is a uniform halo just like that of an isotropic liquid. This is due to the fact that, generally a liquid crystal sample

consists of a large number of domains, the molecules being aligned within each domain in a preferred direction, i.e., the director, but there is no preferred direction for the sample as a whole and naturally, x-ray diffraction pattern has a symmetry of revolution around the direction of x-ray beam.

The principal features of the x-ray pattern of a nematic sample, which is oriented perpendicular to the incident x-ray beam, is shown in the Figures 2.1 (a) and (b). The main halo has split into two crescents for each of which the intensity is maximum in the equatorial direction, i.e., perpendicular to the director (optic axis). These crescents are formed mainly due to the nearest neighbour intermolecular scattering and the corresponding Bragg angle is a measure of lateral intermolecular distance. The angular distribution of the x-ray intensity (Figure 2.1(a)), $I(\psi)$ vs. ψ, also gives the orientational distribution function $f(\cos\theta)$ and order parameters $\langle P_L \rangle$, (L =2,4).

In the meridional direction, at a much smaller Bragg angle, a pair of crescents are also seen. They are connected with apparent molecular length. Sometimes, the inner difuse crescents are replaced by sharp spots and the phase is called " cybotactic nematic phase". In Figure 2.1(b), the four sharp spots arise due to the molecular arrangement within each cybotactic group [20], such that the ends of the molecules constitute well-defined boundary planes which are non orthogonal to the direction of the molecules in the group. This is an example of "skewed cybotactic nematic". In "normal cybotactic nematic" the boundary planes are orthogonal to the director. The tilt angle τ, which is the angle between the molecular long axis and the normal to the plane can be determined from $\tau = (90^{\circ} - \phi/2)$ (Figure 2.1(b)).

The x-ray diffraction pattern from smectic A phase is shown in Figure 2.1(c). The meridional spots are formed due to Bragg

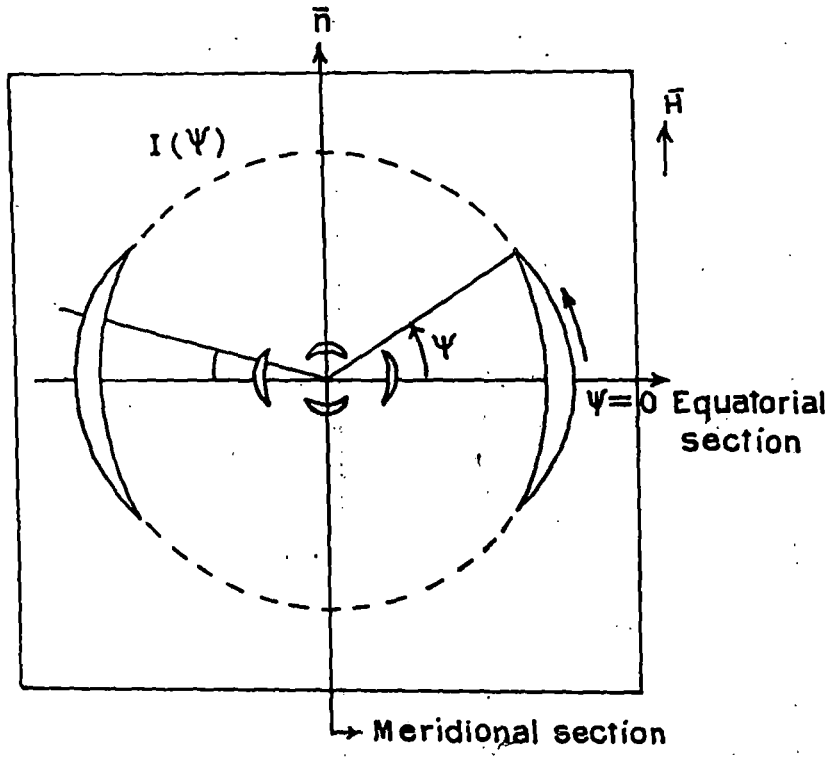

Figure 2.1(a) Schematic representation of the x-ray diffraction pattern of an oriented nematic liquid crystal.

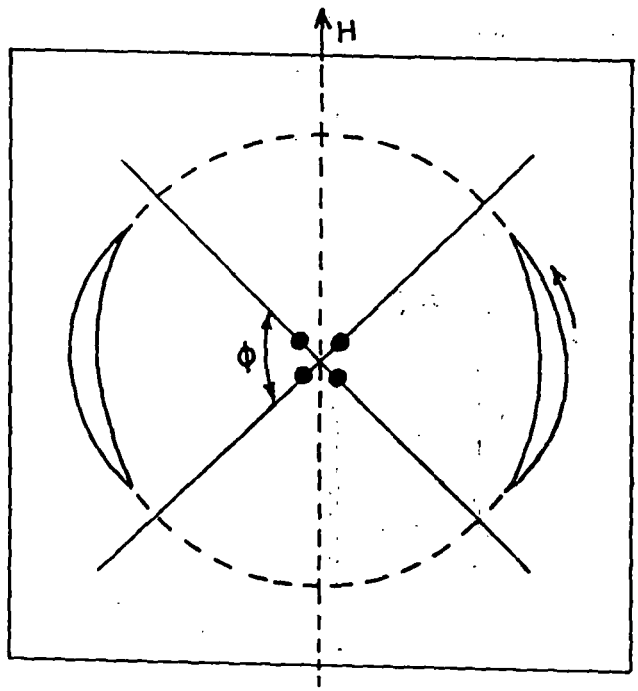

Figure 2.1(b) Schematic representation of the x-ray diffraction pattern of an oriented "skewed cybotactic" nematic liquid crystal.

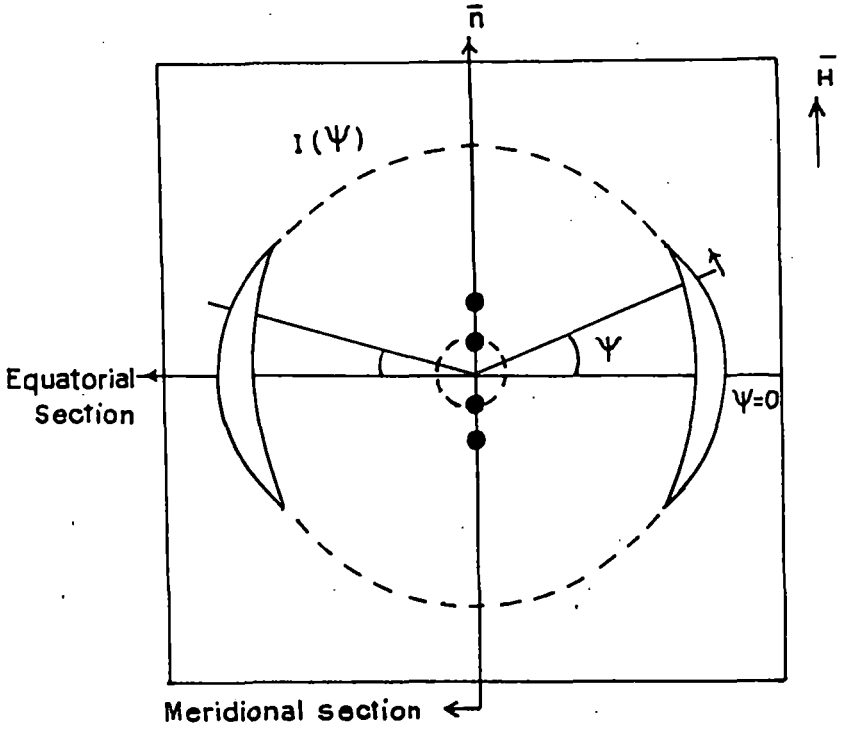

Figure 2.1(c) Schematic representation of the x-ray diffraction pattern of an oriented smectic A liquid crystal.

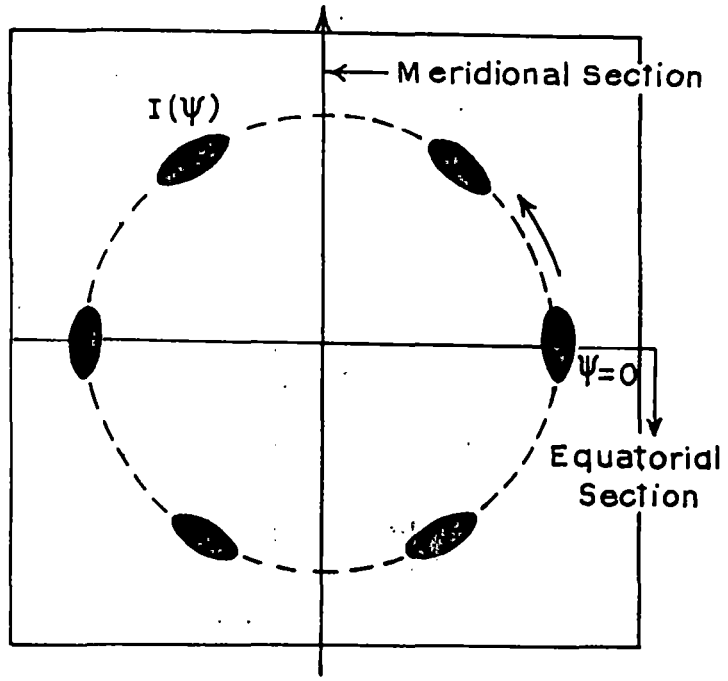

Figure 2.1(d) Schematic x-ray scattering profile for the smectic B phase with the incident x-ray beam parallel to the layer normal.

reflection from the layers and provide the value of the layer thickness. Since the smectic A phase can have only quasi-long range order (QLRO) along its layer normal [3,21], the second order Bragg reflections in the meridional direction are generally very weak and are often absent in the x-ray photographs. When present, these second order reflections provide a method for calculating τ, the translational order parameter.

Figure 2.1 (d) represents the schematic scattering profile for a three-dimentionally ordered system with hexagonal symmetry as in the smectic B phase, with the incident x-ray beam parallel to the layer normal. The outer diffraction ring is split up into six spots of strong intensity. The angular distribution of the x-ray intensity $I(\psi)$ versus ψ gives the measure of the bond orientational order (BOO) within the smectic B phase.

We, also get some faint diffuse rings (crescents) in our x-ray photographs, which may be due to (a) intra molecular atomic scattering, (b) next nearest neighbour intermolecular scattering and (c) effect of white radiation contained in Ni filtered Cu radiation. We are generally not concerned with those diffraction patterns.

2.3.1 Experimental technique and data analysis: x-ray diffraction studies.

X-ray diffraction photographs were obtained with the apparatus described below (Figure 2.2) using nickel filtered CuK_{α} radiation in the transmission geometry on a film [22], using a flat plate camera designed in our laboratory by Jha et al [21]. X- ray diffraction photographs were taken at different temperatures in the presence of a magnetic field. The camera has the provisions to change the collimator (2), spacer (15) and

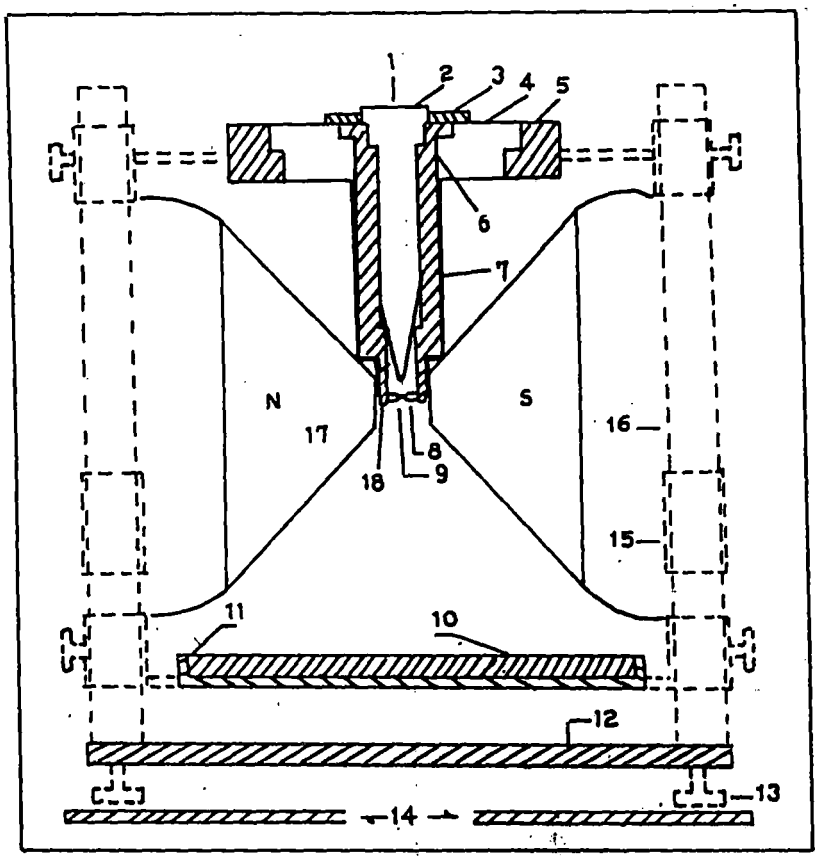

Figure 2.2 Sectional diagram of the x-ray diffraction camera. 1. X-ray 2. Collimator 3. Brass ring 4. Ring of syndanyo board 5. Brass ring 6.Cylindrical brass chamber 7. Asbestos insulation and heater winding 8. Specimen holder and thermocouple 9. Sample 10. Film cassette 11. Film cassette holder 12. Base plate 13. Levelling screw 14. Brass plates over the coils of the electromagnet 15. Removable spacer 16. Supporting brass stand 17. Pole peices 18. Asbestos insulation

sample container (8). The sample was taken in a thin-walled lithium glass capillary of 1 mm diameter. The capillary containing sample was placed inside a brass block. The temperature of the block was controlled within $\pm$ 0.5^{o}C by a temperature controller (Indotherm MD 401). The sample was first heated to the isotropic phase and magnetic field (3 to 6 Kilogauss) was applied parallel to the capillary axis. The substance was allowed to cool to the desired temperature in the presence of the magnetic field. The magnetic field was kept on during the x-ray diffraction experiment. The strength of the magnetic field was measured previously by a gaussmeter (ECIL model GH 867). X- ray beam was collimated by a collimeter of aperture 1 mm. A Ni filter of thickness 0.009 mm was used to obtain predominent CuK_{α} radiation of wavelength 1.5418$\mathring{A}$. When the temperature reached equlibrium then the x-ray tube was switched on. Photographs were taken at various constant temperatures. In case of the determination of orientational order parameters the sample to film distance was maintained at about 5 cm. To obtain better accuracy in the layer thickness measurement, x-ray diffraction photographs of inner spots were taken with sample to film distance increased to about 9 cm.

For the determination of the exact distance between the sample and film I took aluminium-powder photograph. The Bragg angle corresponding to the (hkl) reflecting plane for aluminium can be determined by [23]

$$\sin \theta' = \lambda/2a(h^2 + k^2 + l^2) \qquad 2.12$$

Thus measuring the diameter of the diffraction rings corresponding to (111) and (200) reflections [22] and values of Bragg angles from 2.12, the actual distance between sample and the film can be found out from the relation

$$\tan 2\theta' = \frac{\text{Radius of the ring}}{\text{Sample to film distance}} \qquad 2.13$$

The correction term was then calculated and used to measure the actual sample to film distance, from the apparent distance due to the spacers.

(a). Conversion of optical density to x-ray intensity

The optical density of the x- ray photographs was measured by a microdensitometer (Carl Zeiss MD 100) which has a potentiometric recording (K200) facility for linear scanning. The optical density values obtained from the densitometric scan were converted to relative intensity values by a method explained by Klug and Alexander [24]. An intensity scale was prepared by exposing different portions of a film for different times to x-rays coming through a small rectangular aperture. Multiple film technique was used for smoothening of the calibrated graph. Optical density values of these spots were then measured with the help of microdensitometer. With the front film (first film), an optical density - time in seconds (corresponds to x-ray intensity) graph was drawn. Corresponding to the measured optical densities of the second film, x-ray intensities were recorded from this graph. The average of the ratio's of these intensities corresponding to all the exposures gives the film factor. The intensities of the second film divided by the film factor converts the readings to those of the front film. As the densitometer zeroing was made on unexposed x-ray films, no subtraction for unexposed film optical density was required. The measured O.D. values and corresponding intensities give the film calibration curve as shown in Figure 2.3.

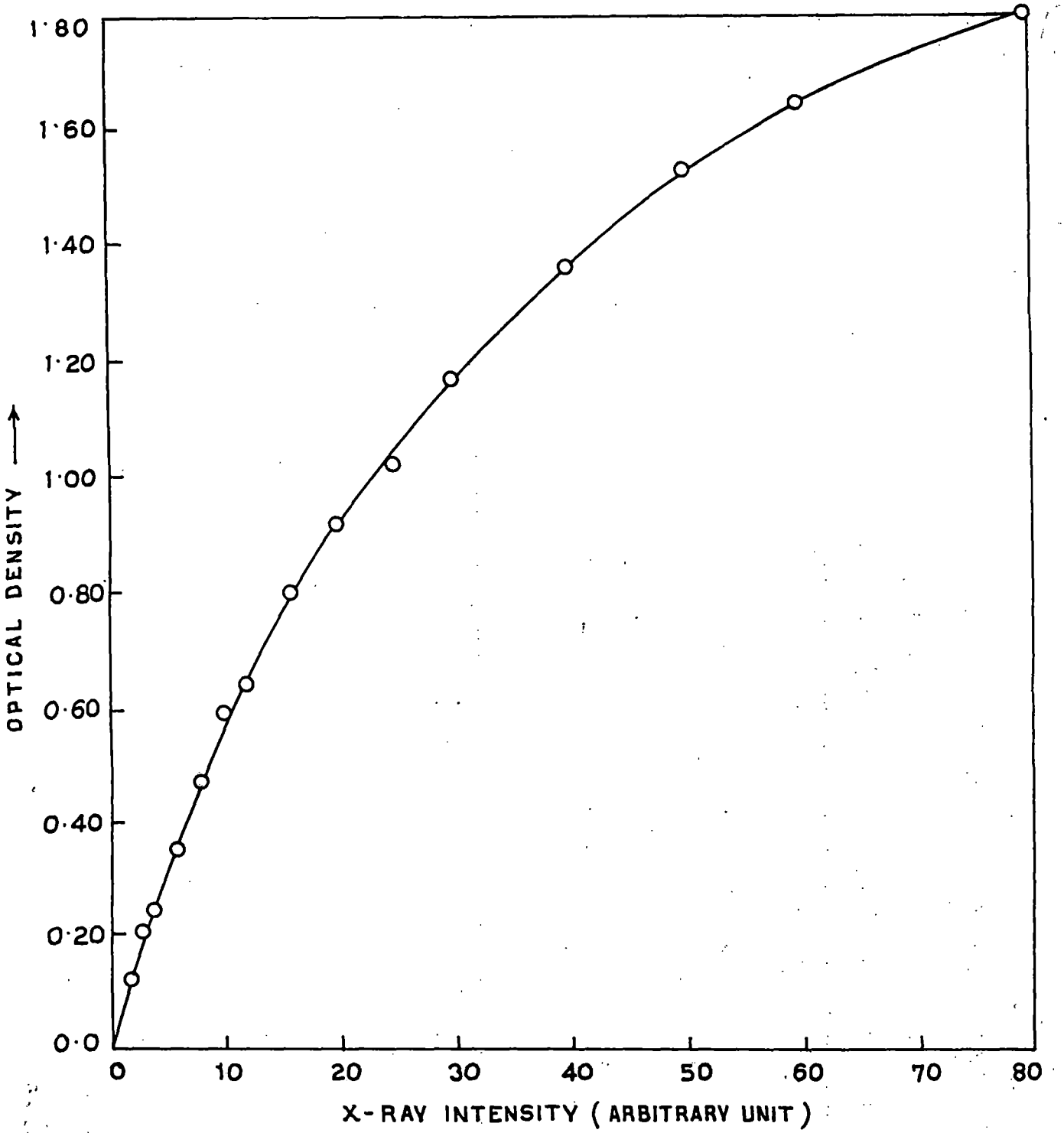

Figure 2.3 Optical density versus x-ray intensity curve used for calibration.

(b). Circular scaning of x-ray photographs

A rotating stage was fabricated by us to facilitate full 360° scanning of the photographs. Photographs were scanned to measure angular intensity distribution $I(\psi)$ which was used to calculate the orientational distribution function $f(\beta)$ and order parameters $\langle P_2 \rangle$ and $\langle P_4 \rangle$. The circular scans of the outer diffraction arc were taken from $\psi = 0$ to $\psi = 360^{\circ}$ at about 1° intervals near the peak and at larger intervals elsewhere. The optical density values obtained from the densitometric circular scan were converted to x-ray intensity with the help of calibration curve. The experimental intensity values were then corrected for background intensity values arising due to the air scattering. The peak intensity position which corresponds to $\psi = 0$ was determined from angle vs. intensity curve (Figure 2.4). Taking nineteen $I(\psi)$ values from $\psi = 0$ to $\psi = 90^{\circ}$ at 5° intervals from the smoothed $I(\psi)$ vs. ψ curve, $f(\beta)$, $\langle P_2 \rangle$ and $\langle P_4 \rangle$ were calculated by using Leadbetter's expression mentioned in later part of this chapter. A computer program has been developed for these calculations.

(c). Linear scaning of x-ray photographs

The diameter of the diffraction rings can be measured from the linear scan of the photographs using the potentiometric recorder and the corresponding optical density vs. linear distance can be plotted.

(d) Deconvolution of x-ray intensities

The experimental x-ray intensity profile were corrected for the finite width of the collimator. Extraction of the pure

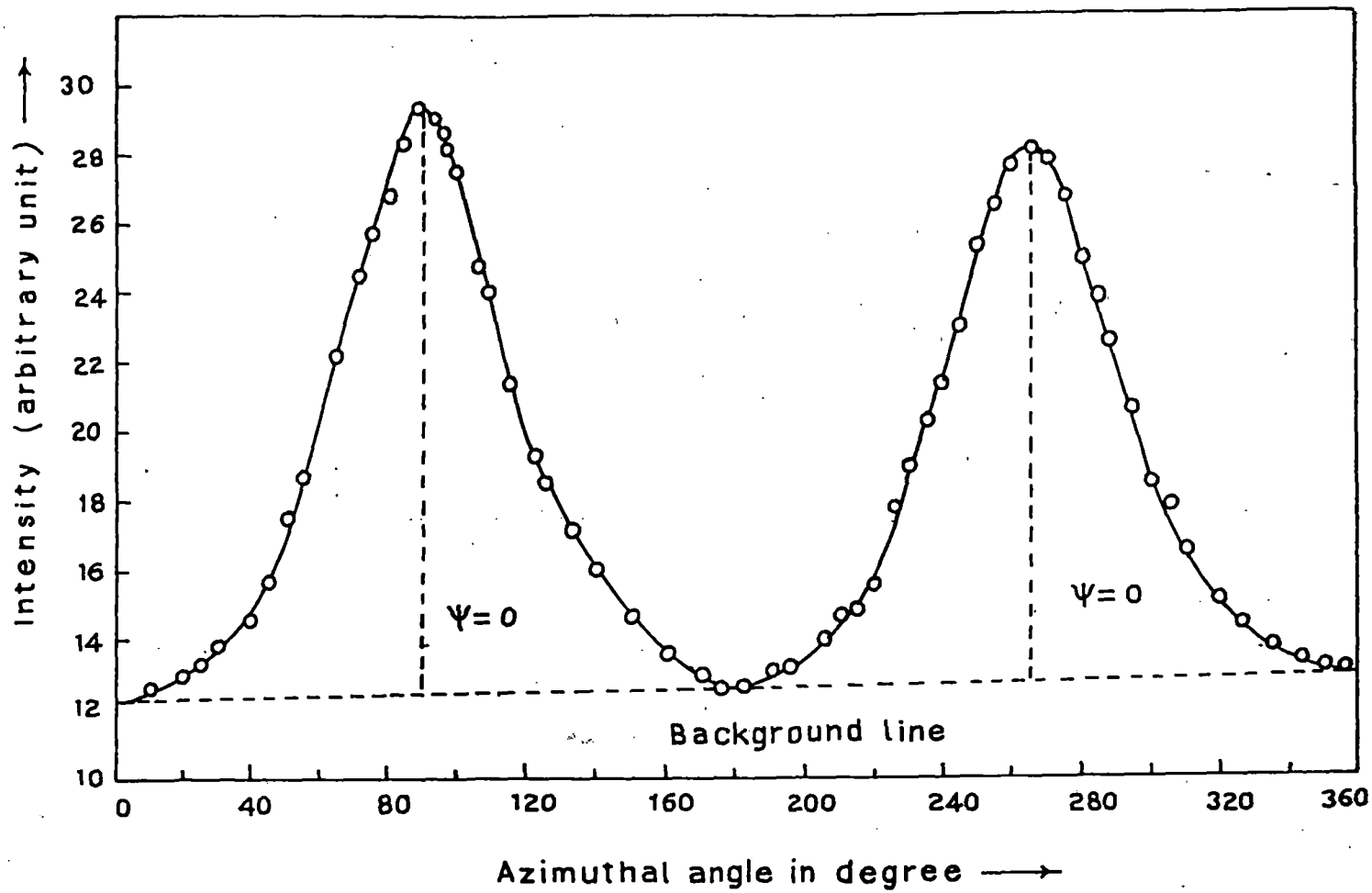

Figure 2.4 Average intensity I(Ψ) versus azimuthal angle (Ψ) curve.

diffraction profile is required for accurate determination of parameters which are affected by the spread of the x-ray diffraction pattern. In this thesis, I have used deconvoluted profiles for the determination of the correlation length ξ and Bond Orientational Order (BOO). For this, I have followed the method of Ergun [25], based on substitution of successive foldings.

The convolution of two integrable functions is defined by,

$$F(s) = \int f(s - u)g(u)du = \int f(u)g(s-u)du \qquad 2.14a$$

where it is assumed that the base domain of integration is the whole s- space. If s is a one dimensional variable, equation 2.14a is termed folding and F(s) is called the fold or convolution of f(s) with g(s). The functions F and g are generally known, the problem is to determine f; this determination is called unfolding or deconvolution. In this case F(s) is the experimentally observed x-ray intensity distribution and g(s) is the intensity distribution of the x-ray beam coming through the collimator. Deconvoluted intensity f(s) is required. As suggested by Ergun [25], the first approximation of the influence of folding is obtained by folding F with g according to equation 2.14a and subtracting the fold of F from F. This difference when added to F yields the first approximation to f and is called the first unfold. The second approximation is obtained by folding the first approximation and adding the difference between F and this second fold to the first approximation. This procedure has been continued until the sum of the absolute values of the difference between F and the fold of n^{th} approximation is minimised. The function g (the intensity distribution of the primary beam), has a bounded support as well as has been normalised i.,e

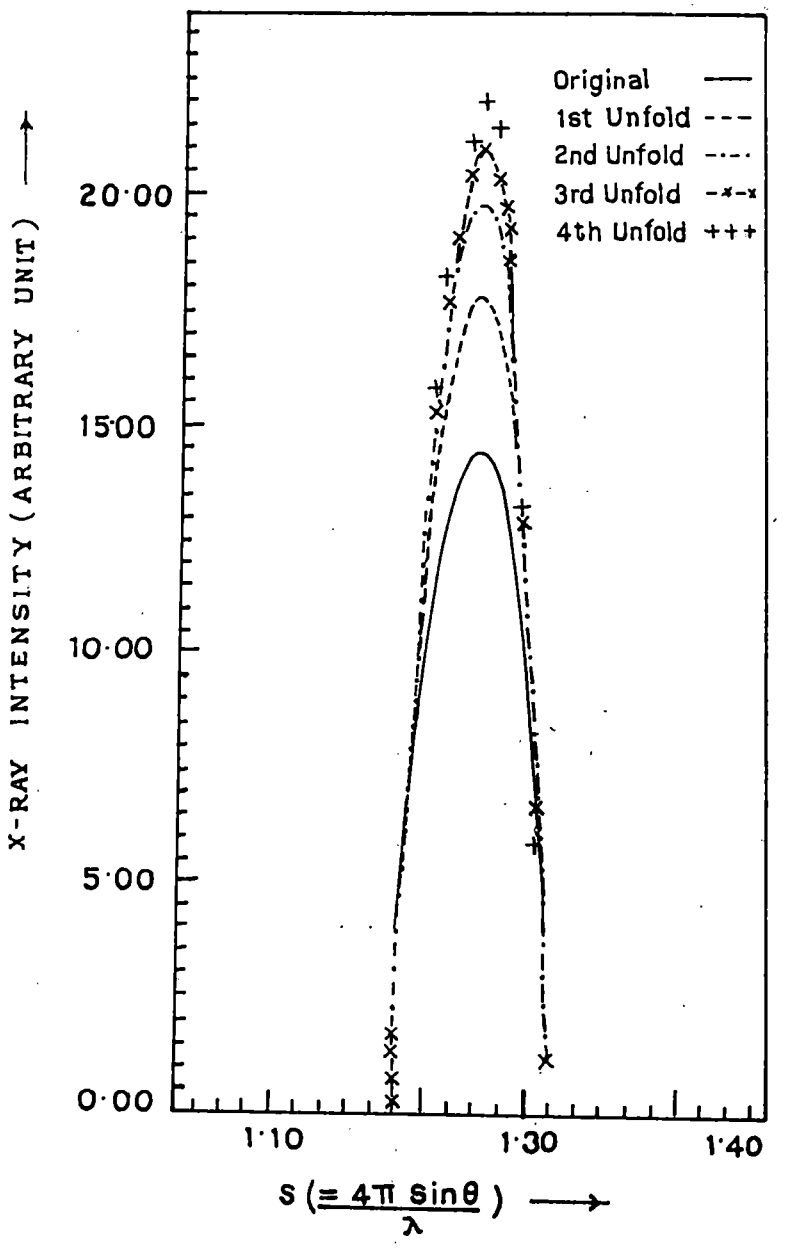

Figure 2.5 The original, first, second, third and fourth unfolded experimental x-ray intensity profile.

$$\int_{-a}^{b} g(u)du = 1 \qquad 2.14b$$

where g(0) corresponds to the value of g at about the midpoint of the primary x-ray beam corresponding to a bragg angle equal to zero. Also, after each iteration the domain of f(s) is reduced by a+b where -a to + b are the limits of the domain of g(u). It has been seen from the width of the primary x-ray beam 3-4 successive foldings are possible. However, as can be seen from Figure 2.5 that the procedure is quite convergent within 3-4 cycles of iteration. A computer programme has been developed for successive foldings and unfoldings where the integrations have been performed numerically by Simpson's Method. The experimental diffraction profile has been often fitted to an analytical form for faster and more convenient numerical integration.

2.3.2 Orientational distribution functions and order parameters

Liquid crystals are characterized by an orientational order of their constituent rod like molecules. The examination of the optical properties of nematic and smectic phases show that they have uniaxial symmetry and the axis of uniaxial (cylindrical) symmetry is parallel to a unit vector $\hat{n}$ called the director. A full description of the orientation of such molecules presupposes a knowledge of the distribution functions. The x-ray pattern of oriented samples consist of equatorial arcs. The distribution of intensity along the diffuse equatorial arcs of x-ray pattern (Figure 2.1a) is related to the distribution function [17].

$$I(\psi) = c \int_{\beta=\psi}^{\pi/2} [\, f_d(\beta)\, \sec^2\psi\, [\, \tan^2\beta - \tan^2\psi\,]^{-1/2} \sin\beta\, d\beta \qquad 2.15$$

where $f_d(\beta)$ is the distribution function for the orientation β for a local cluster of molecules relative to the director $\bar{n}$ (β = 0). The equation (2.15) can be numerically inverted to give $f_d(\beta)$ and are assumed to be close to the singlet distribution function [17].

The orientational order parameters $\langle P_2 \rangle$ and $\langle P_4 \rangle$ were calculated using the relationship

$$\langle P_L \rangle = \int_0^1 P_L(\cos \beta) f_d(\beta) \, d \cos(\beta) \; / \int_0^1 f_d(\beta) \, d \cos(\beta) \qquad 2.16$$

with L = 2, 4

In section 2.3.1a the process of measuring the intensity values $I(\psi)$ from the measured optical densities are discussed. I have calculated the intensity values by angular scanning of the x-ray diffraction photograph for $\psi = 0$ to $\psi = 2\pi$. To calculate $f_d(\beta)$ and order parameter only one quadrant is sufficient. However, I have measured $I(\psi)$ in all the four quadrants separately to calculate $\langle P_2 \rangle$ and $\langle P_4 \rangle$ and obtained almost the same value in each quadrant. Hence, I have used mean $I(\psi)$ (average of four quadrants) values for all calculations reported in this thesis. Errors in order parameter values in this manner are estimated to be $\pm$ 0.02 for both $\langle P_2 \rangle$ and $\langle P_4 \rangle$.

2.3.3 Determination of Bond Orientational Order

The order parameter associated with a system having six-fold symmetry, as in the case of smectic B liquid crystals is the Bond Orientatioanal Order (BOO) [26-29], defined to be the thermal avarage of the quantity

$$\Psi(\vec{r}) = \langle \exp\ (i6\theta(\vec{r}) \rangle \qquad 2.17$$

where the bond angle $\theta(\vec{r})$ is the orientation, relative to any fixed laboratory axis, of a bond between two nearest neighbour molecules. The bond orientational order has been calculated by evaluating the expression,

$$\langle \cos(6\theta) \rangle = \int_0^{\pi/6} \cos(6\theta) f(\theta) d\theta \Big/ \int_0^{\pi/6} f(\theta) d\theta \qquad 2.18$$

where $f(\theta)$ is the angular distribution function of centre of mass of the neighbouring molecules with respect to a central molecule and the angular distribution function has a maximum at $\theta = 0$. Equation 2.18 can be approximated by the following expression,

$$\langle \cos(6\theta) \rangle \approx \int_0^{\pi/6} \cos(6\theta) I(\theta) d\theta \Big/ \int_0^{\pi/6} I(\theta) d\theta \qquad 2.19$$

where $I(\theta)$ is the azimuthal distribution of the x-ray diffraction intensity. Following Vainstein [30] it has been assumed that $I(\theta)$, the intensity distribution, is proportional to $f(\theta)$ the distribution function and consequently has its maximum at $\theta = 0$ also. BOO was calculated for each peak and finally the average over six peaks was taken. The experimental x-ray intensity profile for each peak has been corrected for broadening due to the width of the primary x-ray beam, using a method of deconvolution based on substitution of successive foldings as descibed in section 2.3.1d. The circular scans of the outer diffraction spots (Figure 2.1(d)) was taken from $\psi = 0^{\circ}$ to $\psi = 360^{\circ}$ at 0.5 degree intervals near the peak and at larger intervals elsewhere. The resultant x-ray intensity profile is shown in Figure 2.6 and the peak intensity position

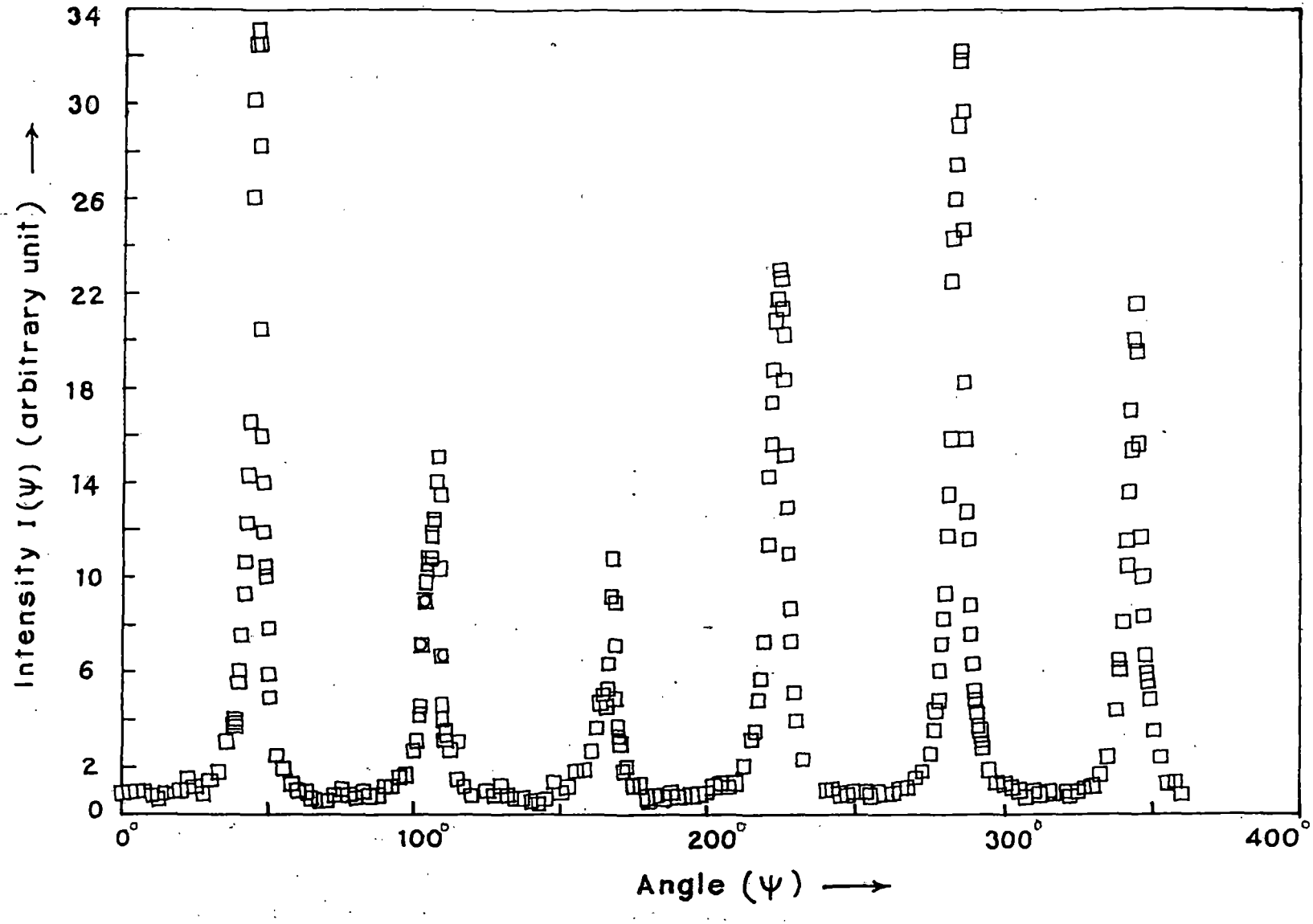

Figure 2.6 X-ray intensity I(ψ) versus azimuthal angle (ψ) curve for the smectic B phase.

corresponding to $\psi = 0$ was determined from this curve following a procedure similar to that followed in the determination of orientational order parameters $\langle P_2 \rangle$ and $\langle P_4 \rangle$. The corrected intensity values plotted against azimuthal angular positions have also been corrected for the background (scattered) intensity values.

2.3.4. Molecular parameters from x-ray studies

(a) Intermolecular distance

The average lateral distance between the neighbouring molecules (D) was calculated from the x-ray diffraction photographs by a formula given by [20]

$$2D \sin \theta = k\lambda \qquad 2.20$$

where 2θ is the Bragg angle for the equatorial diffraction, λ is the wave length of the x- ray and k is a constant which comes from the cylindrical symmetry of the system. Recent calculations [31] have shown that the value of k depends on the order parameter of the sample under consideration. For perfectly ordered state k = 1.117 as given by de Vries [20]. However, since the variation of k with $\langle P_2 \rangle$ is small, I have used the value k = 1.117 for all the calculations.

(b) Apparent molecular length or layer thickness

For apparent molecular length or layer thickness, d, the Bragg equation was used ($2d \sin \theta = \lambda$), where θ is the Bragg angle for the meridional diffraction crescent for an aligned sample or for the inner halo in the case of unaligned samples.

The first order meridional diffraction peaks were used for layer thickness calculation since second order diffraction peaks were either very weak and diffuse or absent.

(c) Transverse correlation length

The transverse (i.e., perpendicular to the director) correlation lengths in both nematic and smectic phases have been determined from the linear scan of outer x-ray diffraction peaks along the equatorial direction. The x-ray intensity profile was first corrected for the use of a flat plate camera following the inverse square law relation. The intensity profile was then deconvoluted for finite width of the collimator. The corrected x-ray intensity profile I(q) in the transverse q(wave vector) direction was fitted using a least-squares method to the Lorentzian form with a quadratic background:

$$I(q) = \frac{a}{b + (q - q_o)^2} + cq^2 + dq + e \qquad 2.21$$

where a, b, q_o, c, d and e are adjusted to obtain the best fit. A computer programme using Lavenberg - Marquardt method [32a] was written for this non-linear least squares fitting, initial values of the parameters being estimated graphically. Convergence was found to be good for all the experimental intensity profiles. The value of q_o gives the position of the x-ray diffraction peak and correlation length ξ is equal to $2\pi(b)^{-1/2}$. As mentioned in section 2.3.1d, in the deconvolution procedure an analytical form for the experimental intensity profile is helpful in the numerical integration process. Thus, I have first fitted the experimental data to a lorentzian form with a quadratic background, as shown in Figure 2.7(a). Figure

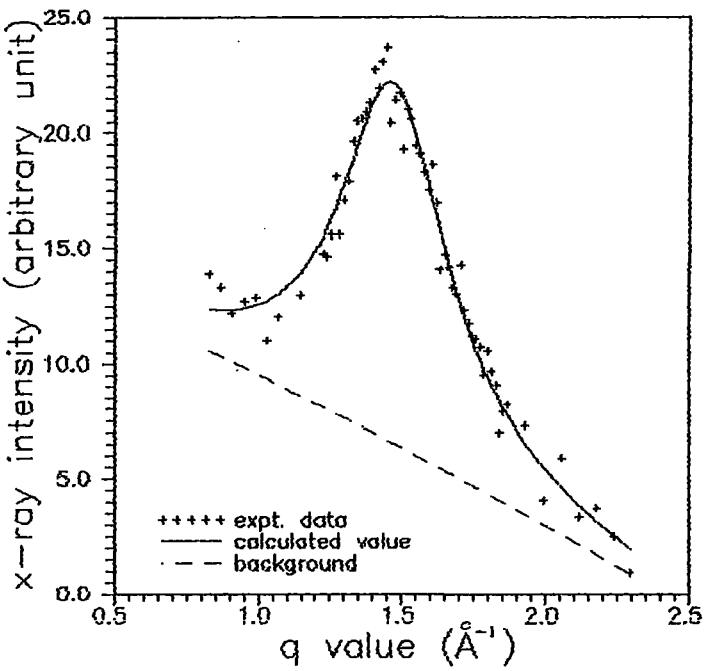

Fig.2.7a Comparison of experimental x-ray intensity data with the calculated value; HAB at 85 deg C.

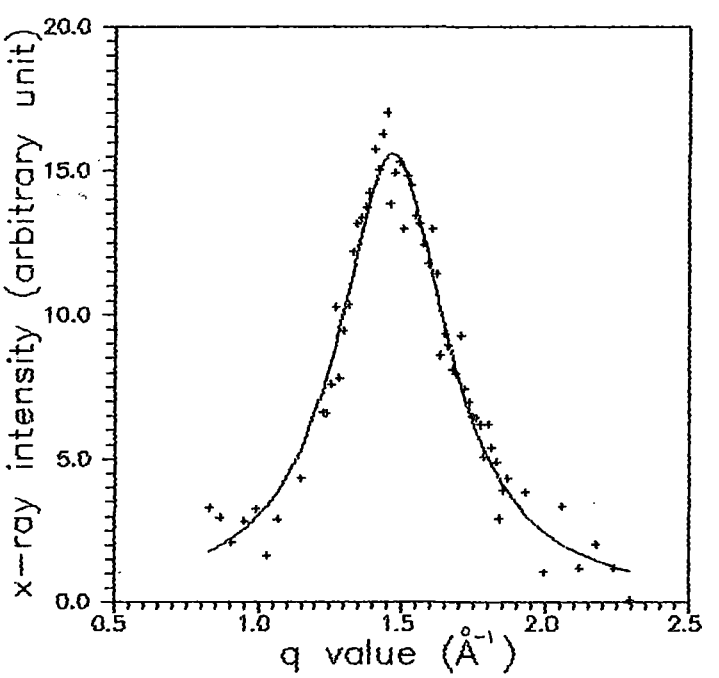

Fig.2.7b Comparison of x-ray intensity obtained from calculated peak value with experimental peak value after substracting the background;HAB at 85 deg C;solid line calculated peak; + expt. intensity minus calculated background.

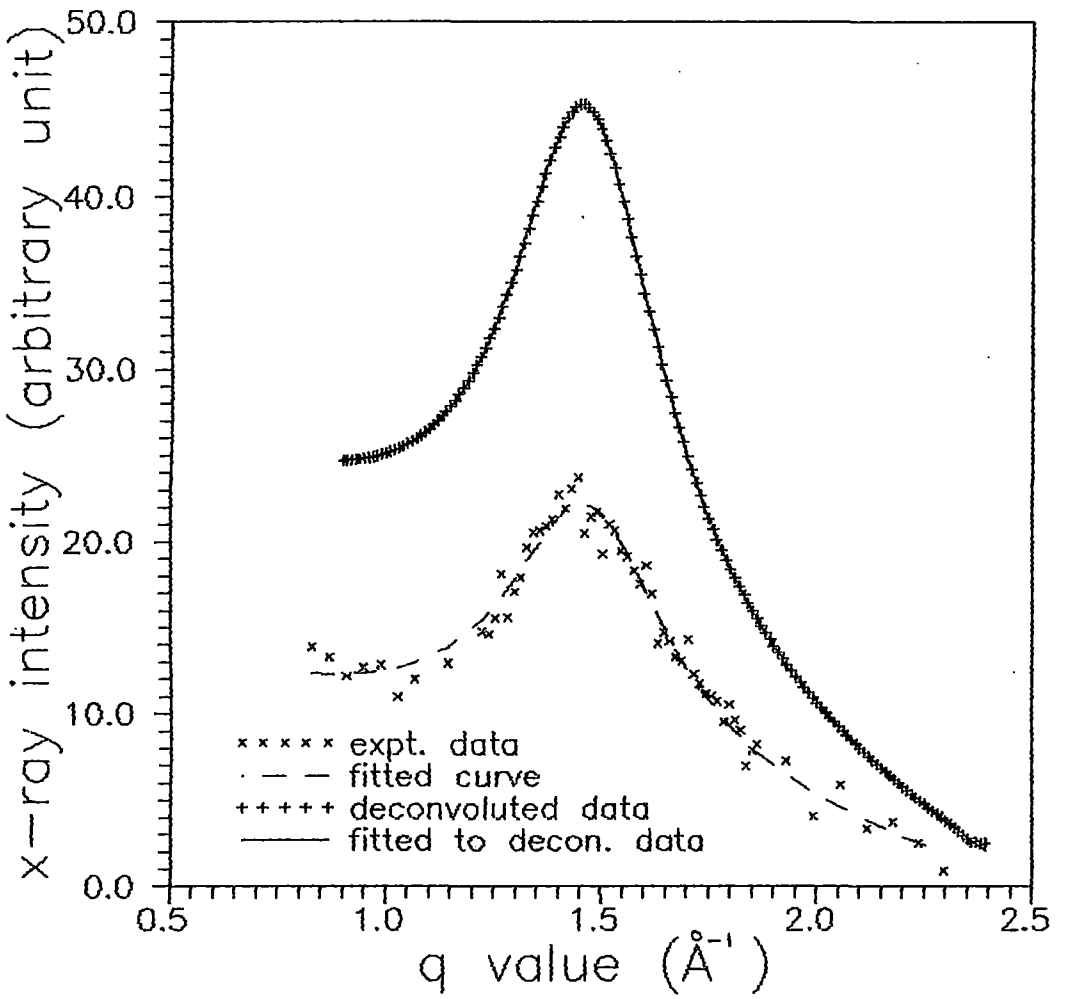

Fig.2.7c Comparison of experimental x-ray intensity data before and after deconvolution; HAB at 85 deg C.

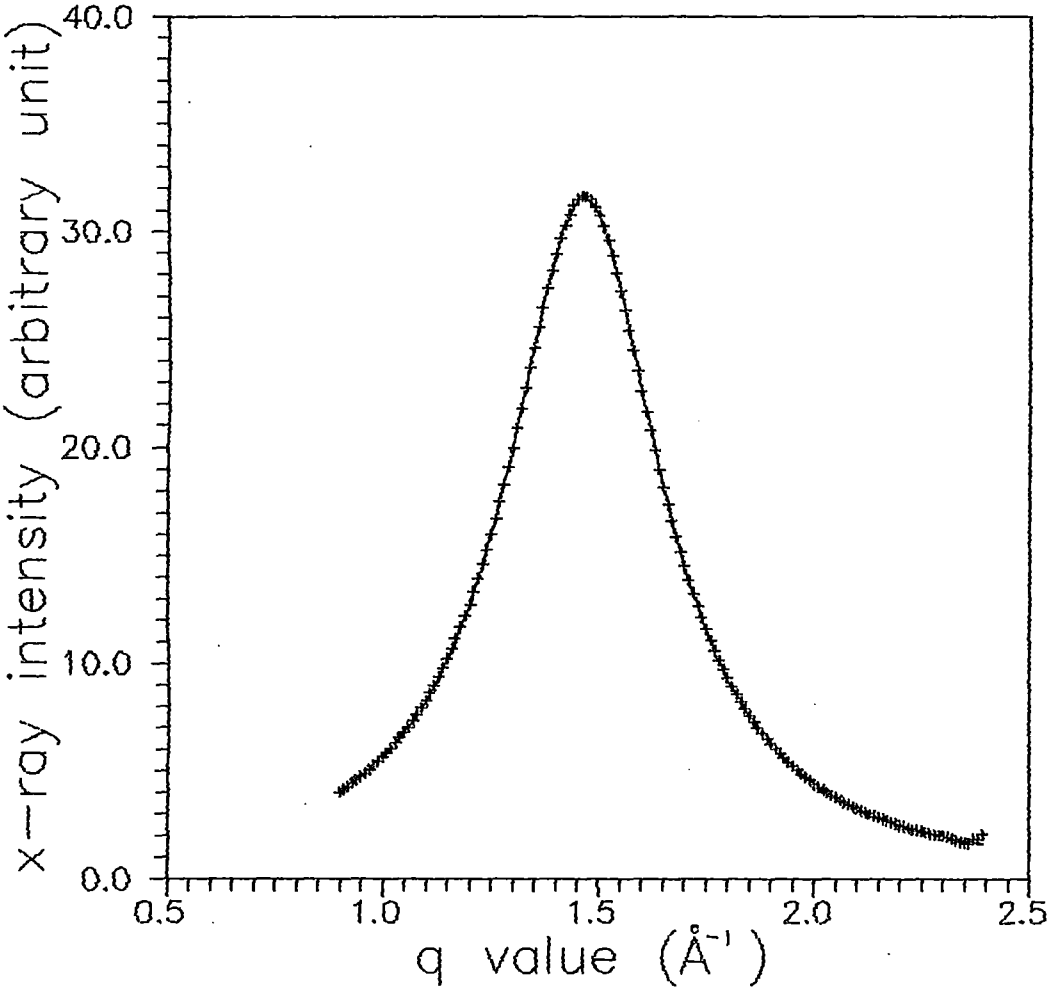

Fig. 2.7d Comparison of x-ray intensity obtained from calculated peak value with experimental peak value after substracting the background; HAB at 85 deg C; solid line calculated peak;+ expt. intensity minus calculated background.

2.7b shows the calculated profile as obtained from this fitting to the experimental data after substracting the background. Figure 2.7c shows the deconvoluted peak (after 3 to 4 iterations) fitted to the form given in eqaution 2.21 together with the experimental x-ray intensity data prior to deconvolution. The calculated peak after substraction from the background is shown in Figure 2.7(d). It can be seen from Figure 2.7c that the deconvoluted intensity data fit extremely well with the Lorentzian form.

2.4 Refractive index of mesophases

Anisotropic crystals (and also aligned liquid crystals) produce double refraction and the ability of a crystal to separate the two refracted rays is measured by its birefringence. In liquid crystalline phases refractive indices are important parameters for technical application. The first birefringence measurements were made by E. Dorn [32], the theoretical explanation of which have given by O. Weiner [33]. and H. Zocher [34,35]. The refractive indices of large number of nematic liquid crystals have been investigated, I refer here some of the earlier works [36-42]. Refractive indices have also been investigated in smectic phases [43-45]. In liquid crystals, due to the anisotropic molecular arrangement, it is necessary to take into account the effect of the anisotropic internal field in evaluating the polarizabilities. Hence, in case of liquid crystals the well known Lorentz - Lorentz formula for isotropic media is generally replaced by Neugebauer's [46] relations or Vuk's formula [47]. Saupe and Maier [48] also applied a more elaborate form of internal field suggested by Neugebauer.

In this study, I have measured the ordinary and extraordinary refractive indices n_o and n_e for different liquid crystal samples

and have calculated the effective polarizabilities α_o and α_e of anisotropic liquid crystals by using the two different internal field models [46,47]. Finally orientational order parameter $\langle P_2 \rangle$ was calculated.

(a) Neugebauer's method

Neugebauer [46] extended Lorentz - Lorentz equations for an isotropic system to an anisotropic system. In this model, Neugebauer calculated the anisotropy of internal field by considering an arbitrary lattice in which the molecules are represented by anisotropic point polarizabilities with parallel principal axes. The effective polarizabilities α_e and α_o of the liquid crystals are given by,

$$n_e^2 - 1 = 4\pi N\alpha_e \left(1-N\alpha_e\gamma_e\right)^{-1} \qquad 2.22$$

$$n_o^2 - 1 = 4\pi N\alpha_o \left(1- N\alpha_o\gamma_o\right)^{-1} \qquad 2.23$$

where γ_i's are the respective internal field constants for ordinary and extraordinary rays, N is the number of molecules per c.c and n_e and n_o are the extraordinary and ordinary refractive indices respectively. The equations for calculating the α_o and α_e obtained from equations (2.22) and (2.23) are

$$\frac{1}{\alpha_e} + \frac{2}{\alpha_o} = \frac{4\pi N}{3}\left[\frac{n_e^2 + 2}{n_e^2 - 1}\right] + \left[\frac{2(n_o^2 + 2)}{n_o^2 - 1}\right] \qquad 2.24$$

and

$$\alpha_e + 2\alpha_o = \frac{9}{4\pi N}\left[\frac{n^2 - 1}{n^2 + 2}\right], \qquad 2.25$$

where $n^2 = 1/3\ (n_e^2 + 2n_o^2)$.
Solving equations 2.24 and 2.25 α_o and α_e values can be obtained.

(b) Vuks Method

Vuks has derived another formula for polarizabilities associated with anisotropic organic molecules, by assuming that the internal field is independent of orientation i.e. an isotropic system with different polarizabilities. The principal polarizabilities and refractive indices can be expresssed as

$$\frac{n_e^2 - 1}{\bar{n}^2 + 2} = \frac{4\pi N}{3}\alpha_e \qquad 2.26$$

$$\frac{n_o^2 - 1}{\bar{n}^2 + 2} = \frac{4\pi N}{3}\alpha_o \qquad 2.27$$

where $\bar{n}^2 = \frac{1}{3}\ (n_e^2 + 2n_o^2)$ is the mean refractive index and α_e and α_o can be calculated directly from the refractive index values.

2.4.1. Calculation of order parameters from polarizabilities

The principal polarizabilities (α_o,α_e) have been calculated by using Vuks' isotropic model and Neugebauer's relations (anisotropic model). The relation between the order parameter, $\langle P_2 \rangle$ and the polarizabilities (α_o,α_e) is given by de Gennes [49],

$$\alpha_e = \bar{\alpha} + \frac{2}{3}\alpha_a \langle P_2 \rangle \qquad 2.28$$

$$\alpha_o = \bar{\alpha} - \frac{1}{3}\alpha_a \langle P_2 \rangle \qquad 2.29$$

and

$$\langle P_2 \rangle = \frac{\alpha_e - \alpha_o}{\alpha_{\parallel} - \alpha_{\perp}} \qquad 2.30$$

where $\bar{\alpha} = (2\alpha_o + \alpha_e)/3$ is the mean polarizability. $\alpha_a = (\alpha_{\parallel} - \alpha_{\perp})$ is the molecular polarizability anisotropy where $\alpha_{\parallel}$ and $\alpha_{\perp}$ are the principal polarizabilities, parallel and perpendicular to the long axes of the molecules in the crystalline state, which are not however available experimentally. To get the values of $(\alpha_{\parallel} - \alpha_{\perp})$ the widely used method of Haller et al [50] was adopted. A graph was plotted with $\log(\alpha_e - \alpha_o)$ versus $\log(T_c - T)$, where T_c corresponded to the nematic isotropic transition temperature. The plot which is found to be a straight line is extrapolated to T = 0, giving $(\alpha_e - \alpha_o)_{T=0} = (\alpha_{\parallel} - \alpha_{\perp})$. For each case a set of values of α_e, α_o and $(\alpha_{\parallel} - \alpha_{\perp})$ were obtained and then from equation 2.30 order parameter $\langle P_2 \rangle$ was calculated.

2.4.2 Measurement of refractive indices

The refractive indices n_e and n_o for extraordinary and ordinary ray were measured by a thin prism technique. The refracting angle of the prism was less than 2^o. The details of the preparation of the prism and the experimental procedure have already been reported by Zemindar et al [51]. For the preparation of a prism two clean optically plane glass plates were used, one surface each of the glass plates was rubbed parallel to the direction of one of their edges. The plates were then treated with a dilute solution of polyvinyl alcohol and

then dried. The preferred direction on the substrate can be obtained by rubbing the same surface in the same direction again by a tissue paper. The prism was then formed by placing the treated surfaces inside with the rubbing direction parallel to the refracting edge of the prism. A thin spacer was placed at the thick edge of the prism for getting the desired refracting angle of the prism. The sides of the prism were sealed with a high temperature adhesive. Liquid crystal sample was placed inside through open top side of the prism and heated to the isotropic state and then cooled down very slowly and the process was repeated several times. No magnetic field was applied. Repeated heating and cooling produced a homogeneous sample with optic axis parallel to the refracting edge of the prism. The prism was then placed in a brass chamber, with transparent windows, whose temperature could be maintained by a temperature controller (Indotherm model 401) at any desired value to an accuracy of $\pm$ 0.5^{o}C by means of an electric oven. The refractive indices were measured for three wavelengths (λ = 6907$\mathring{A}$, 5890$\mathring{A}$, 5461$\mathring{A}$) from a mercury lamp by means of a precision spectrometer, a wavelength selector and a nicol prism.

2.5 Measurement of Densities

The densities of the liquid crystals were measured with the help of a dilatometer of the capillary type. A weighed sample of the liquid crystal was introduced inside the capillary tube of the dilatometer and it was placed in a thermostated water bath. Sufficient time was allowed for equilibrium at any desired temperature before taking each readings. The length of the liquid crystal column was measured at different temperatures with a travelling microscope. The densities were calculated after correction for the expansion of the glass. The accuracy of

the measurement of the densities was within 0.1%.

2.6 Elastic Constant and deformation free energy of nematic liquid crystal

Many of the important physical properties involving the response of the bulk liquid crystal samples can be described by regarding the liquid crystal as a continuous medium. Based on this point of view , Zocher [52], Oseen [53] and Frank [54] developed a phenomenological continuum theory which can explain various field induced effect of liquid crystals.

The elastic constants of a liquid crystal are restoring torques which become apparent when the system is perturbed from its equilibrium configuration. As shown by Zocher [52], Osceen [53] Frank [54] the elastic part of the internal energy density of a pertubed liquid crystal is given by the equation :

$$F_{def} = (1/2)\ [K_1(\mathrm{div}\hat{n})^2 + K_2(\hat{n}.\mathrm{curl}\hat{n})^2 + K_3(\hat{n}\times\mathrm{curl}\hat{n})^2] \qquad 2.31$$

where K_1, K_2, K_3 refers to the splay, twist and bend elastic constants respectively and $\hat{n}$ is the director (Figure 2.8).

2.6.1 Freedericksz transition

Various methods have been used to measure the elastic constants of nematic liquid crystals. One of the most simple and convenient method is Freedericksz transition, where an external electric [55-58] or magnetic [59-66] field is applied to deform a thin layer of surface aligned nematogenic sample having uniform director pattern. Below a critical field the sample remains surface aligned, but above it starts to align itself along the external field for nematogens having positive

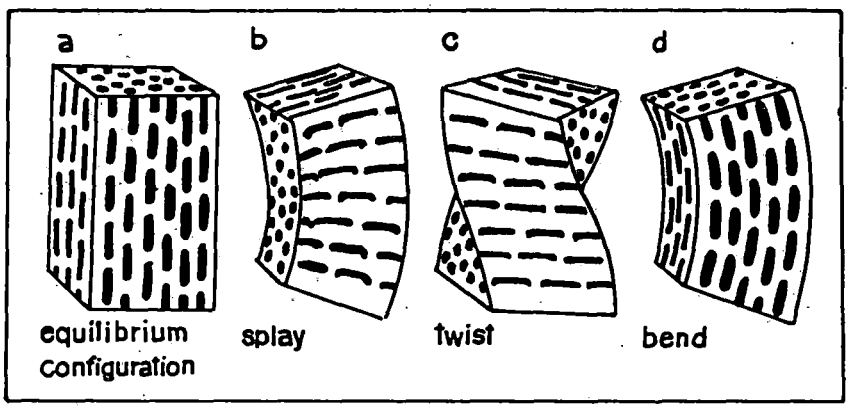

Figure 2.8. (a) An ordered liquid crystal in equilibrium configuration. The deformation states —— splay (b), twist (c) and bend (c) [67].

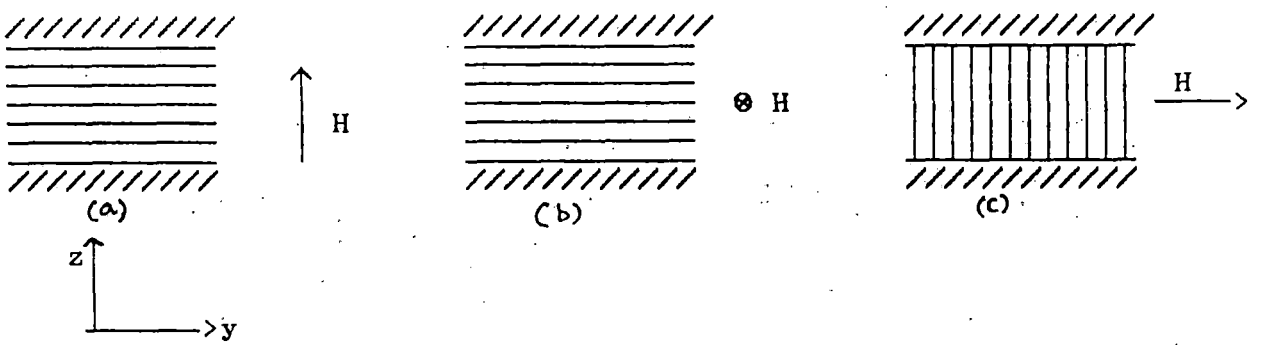

Figure 2.9 Schematic experimental set-up for the determination of elastic constants from Freedericksz transition: (a) splay, (b) twist, (c) bend.

anisotropy ($\Delta\chi > 0$ or $\Delta\varepsilon > 0$). This phenomenon is known as Freedericksz's transition. Depending on the geometry of the arrangement, splay, twist or bend elastic constant can be determined from Freedericksz transition in a magnetic field as shown in Figure 2.9. The threshold magnetic field for all the three geometries can be obtained in a generalised form as

$$(H_C)_i = (K_i/\Delta\chi)^{1/2} \frac{\pi}{d} \qquad 2.32$$

i = 1,2,3 refer to the splay, twist and bend deformations respectively, d is the thickness of the liquid crystal layer, $\Delta\chi$ is the diamagnetic anisotropy. and $(H_c)_i$ is the respective critical magnetic field.

2.6.2 Description of experimental setup for determination of K_1 and K_3.

A block diagram of the experimental setup for studying elastic constants by Freedericksz transition method is shown in Figure 2.10.The monochromatic light beam (sodium D light) is incident on the sample, which is mounted in a brass oven (o), after passing through a lens (L), polarizer (P) and collimating circular slits (C_1, C_2). The temperatures are measured and regulated with an accuracy $\pm$ 0.5^{o}C with the help of a thermocouple inserted in the block containing the sample and a temperature regulator (Indotherm model 457). The transmitted light intensity is detected by a photomultipier tube (M) for photon counting. An analyser is placed in front of the P.M. tube. The polariser and analyser are placed in crossed position. The magnetic field H is applied perpendicular to the direction of the preferred orientation of the liquid crystal sample. The

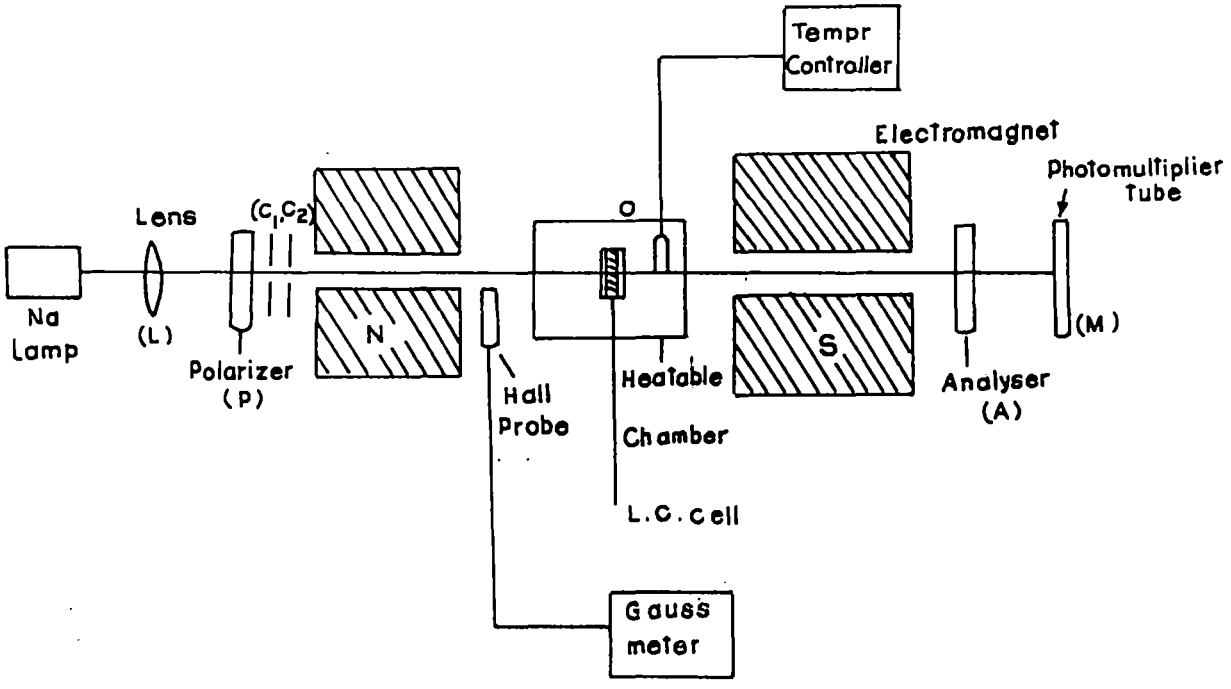

Figure 2.10. Block diagram of the experimental set - up for measuring elastic constants by Freedericksz transition.

field is changed slowly so that the nematic orientation remain in equlibrium with the applied magnetic field. The intensity of the transmitted light is measured as a function of the applied magnetic field for any desired temperature. It is observed that when the field H reaches a critical value H_c the optical properties of the sample change drastically and thus value H_c can be measured from field versus intensity curve within an accuracy of ± 10 gauss. The magnetic field is measured by a sensitive Gaussmeter(Model DGM-102). For the determination of actual threshold it is necessary to maintain the direction of the director exactly normal to the applied magnetic field.

The sample is taken between two plane parallel glass plate separated by a teflon spacer of thickness 50μm. The glass plates are cleaned by different cleaning agent and subsequently dried and treated for homeotropic or homogeneous alignment as required (details of the technique has been given by de Jeu [52]). The splay elastic constant (K_1) is measured using cells with homogeneous planar alignment where inside surface of the glass plates are treated with 1.0% aquous solution of polyvinyl alcohol, dried and then rubbed unidirectionally with tissue paper. In case of bend elastic (K_3) constant measurement it is necessary to treat the glass plates with dilute solution of cetyl trimethyl ammonium bromide in acetone to get homeotropic alignment and using the geometrical arrangement shown in Figure 2.9(c).

Actually, the experiment for the determination of K_1 and K_3 consists of measuring the variation of birefringence of light incident normal to the liquid crystal film. A linealy polarized light incident on the film and the suitable analyser C (i.e., a combination of quater wave ($\lambda/4$) plate and a linear polariser) is used to detect the transmitted light intensity. When the fields exceeds a critical value H_C the transmitted intensity

shows a sudden change. If the field is gradually increased further, the intensity exhibits oscillations because of the change of the phase retardation.

The threshold field for twist deformation cannot be detected optically when viewed along the twist axis. The large birefringence of the medium for this direction of propagation, the state of polarization of the transmitted beam is indistinguishable from that of the emerging beam from the untwist nematic. A total internal reflection technique can be used to measure the K_2 values of the twist deformation. However, I have measured only K_1 and K_3 values at different compositions of a binary liquid crystalline mixture.

REFERENCES

[1]. E.B. Priestley, P.J.Wojtowicz and P. Sheng, eds. Introduction to Liquid Crystals, Plenum, New York, (1974).

[2]. S. Chandrasekhar, Liquid Crystals, Cambridge University Press, Cambridge,(1977).

[3]. G. Vertogen and W.H. de Jeu, Thermotropic Liquid Crystals, Fundamentals, Springer-Verlag (1988).

[4]. G.R. Luckhurst and G.W. Gray, (Editors) The Molecular Physics of Liquid Crysals, Academic Press (1979).

[5]. P. G. de Gennes, The Physics of Liquid Crystal, Clarendon Press, Oxford,(1974).

[6]. A. Saupe and W. Maier Z. Natureforsch, 14a, 882 (1959) and 15a, 287 (1960).

[7]. W.L. McMillan, Phys. Rev., A4, 1238 (1971).

[8]. W.L. McMillan, Phys. Rev., A6, 936 (1972).

[9]. E.B. Priestley, P.S. Pershan, R.B. Meyer and D.H. Dolphin, Vijnana Parishad Anusandhan Patrika 14, 93 (1971).

[10]. K.K. Kobayashi, J. Phys., Soc. (Japan), 29, 101 (1970).

[11]. K.K. Kobayashi, Mol. Cryst. Liq. Cryst., 13, 137 (1971).

[12]. D. Demus and L. Richter, Textures of Liquid Crystals, Verlag Chemie, New York (1978).

[13]. Advances in Liquid Crystals, Vol 6, Ed. G.H. Brown Academic Press (1983), Chapter 1.

[14]. B.K. Vainstein and I.G. Chistyakov, Problems of Modern Crystallography, Nauka, Moscow (1975).

[15]. A.J. Leadbetter, The Molecular Physics of Liquid Crystals, Eds. G. R. Luckhurst & G.W. Gray, Chapter 13, Academic Press (1979).

[16]. A. de Vries, Liquid Crystals, Ed. F.D. SAeva, M. Dekker Inc., New York.

[17]. A.J. Leadbetter and E.K. Norris, Mol. Phys.,38, 669

(1979).

[18]. A. de Vries J. Chem. Phys., 56, 4489 (1972).

[19]. H. Kohli et al Z. Physik, B24, 147 (1976).

[20]. A.de Vries, Mol. Cryst. Liq. Cryst, 10, 219 (1970).

[21]. P.S. Pershan, Structure of Liquid Crystal Phases, World Scientific (1988).

[22]. B. Jha and R. Paul, Proc. Nucl. Phys. Solid State Phys. Symp., India, 19c, 491 (1970).

[23]. C. Kittle, Int. to Solid State Phys, Wiley Eastman, Ch.2 (1976).

[24]. H.P. Klug and L.E. Alexander, X-ray diffraction procedures, John Wiley and Sons, N Y, Page 114 and 473 (1974).

[25]. S. Ergun, J. Appl. Cryst. 1, 19 (1968).

[26]. C.C. Huang in K.J. Standburg (Ed.) Bond Orientational Order in Condensed Matter Systems, Springer - Verlag.

[27]. R. Bruinsma and D.R. Nelson, Phys. Rev. B., 23, 1, 402 (1981).

[28]. E. Gorecka, Li Chen, O. Lavrentovich and W. Pyzuk, Europhysics Letters, 27(7), 507, 1994.

[29]. R.J. Birgeneau and J.D. Litster, J.Phys. Letts. 39, L399, (1978).

[30]. B.K. Vainstein, Diffraction of X- rays by Chain Molecules, Elsevier, Pub. Co. (1966).

[31]. R. Paul. and G. Chaudhuri, Abstract in the 14th International Liquid Crystal Conference, Pisa, 1992, Abs-no-H- P23.

[32]. E. Dorn, Z. Physik, 11, 111 (1910).

[32a].W.H. Pness, S.A. Teukolsky, W.T. Vellering and B.P. Flannery, Cambridge University Press, 1986, Chapter 15.

[33]. O. Weiner, S. Ber. Sächs. Ges. Wissensch., 61, 113 (1909).

[34]. H. Zocher, Naturwiss., 13, 1015 (1925).

[35]. H. Zocher, Z. Krist.,79, 122 (1931).

[36]. F. Grandjean, Compt. rend., 168, 408 (1919).

[37]. N.V. Madhusudana, R. Sashidhar and S. Chandrasekhar, Mol. Cryst. Liq. Cryst., 13, 61 91971).

[38]. Y.Poggi, J. Robert and J. Borel, Mol. Cryst. Liq. Cryst. 29, 31 (1975).

[39]. R Chang, Mol. Cryst. Liq. Cryst., 30, 155 (1975).

[40]. C.C. Huang, R.S. Pindak and J.J. Ho, J. Phys. Lett (Paris), 35, 185 (1974).

[41]. W. Kuczynski and B. Stryla, Mol. Cryst. Liq. Cryst., 31, 267 (1975).

[42]. M. Laurent and R. Journeaux, Mol. Cryst. Liq. Cryst., 36, 171 (1976).

[43]. G. Pelzl and H. Sackmann, Mol. Cryst. Liq. Cryst., 15, 75 (1971).

[44]. G. Pelzl and H. Sackmann, Symp. Faraday Soc., No. 5, 68, (1971).

[45]. Y. Galerne, S.T. Lagerwall and I.W. Smith, Opt. Commun., 19, 147 (1976).

[46]. H. E. Neugebauer, Canad. J. Phys., 32, 1 (1954).

[47]. M. F. Vuks, Optics and Spectroscopy, 20, 361 (1966).

[48]. A. Saupe and W. Maier Z. Natureforsch, 16a, 816 (1961).

[49]. P.G. de Gennes,. Mol. Cryst. liq. Cryst, 12, 193 (1971).

[50]. I. Haller, H.A. Huggins, H.R. Lilienthal and T.R. McGuire, J. Phys. Chem.,77, 950 (1973).

[51]. A.K. Zeminder, S. Paul and R. Paul, Mol. Cryst. Liq. Cryst., 61, 191 (1980).

[52]. H. Zocher, Trans Faraday Soc., 29, 945 (1933).

[53]. C.W. Oseen, Trans Faraday Soc., 29, 883 (1933).

[54]. F.C. Frank, Faraday, Soc. Discussion 25, 19 (1958).

[55]. H. Gruler, T.J. Schiffer and G. Meier, Z. Natureforsh, 27a, 966 (1972).

[56]. H. Gruler and L. Cheung, J. Appl. Phys. 46, 5097 (1975).

[57]. H. Deuling in Liquid Crystals, Solid State Physics Suppl. no. 14, ed. L. Liebert p.77, Academic Press (New York).

[58]. M.J. Bradshaw and E.P. Raynes, Mol. Cryst. Liq. Cryst., 72, 35 (1980).

[59]. V. Freedericksz and V. Tsvetkov, Phy. Z. Soviet Union, 6, 490 (1934).

[60]. V. Freedericksz and V. Zolina, Trans. Faraday Soc. 29, 919 (1933).

[61]. P.P. Karat and N.V. Madhusudana, Mol. Cryst. Liq. Cryst., 40, 239 (1977).

[62]. H.P. Schad and M.A. Osman, J. Chem. Phys. 75 (2) 880 (1981).

[63]. F. Leenhouts, H.J. Boeber, A.J. Dekker and J.J. Jonker, J. Phys. (Paris) Colloque 40, C3-291 (1979).

[64]. H.P. Schad, G. Bauer and G. Maier, J. Chem. Phys. 67, 3705 (1977).

[65]. F. Leenhouts and A. J. Dekker, J. Chem Phys, 74, 1956 (1981).

[66]. H.P. Schad and M.A. Osman, J. Chem. Phys. 75 (2) 880 (1978).

[67]. L. Pohl and U. Finkenzeller in B. Bahadur (Ed.) Liquid Crystals, Applications and Uses, Vol 1. World Scientific p. 166, (1990).